Registration of the endoluminal surfaces of the colon derived from prone and supine CT colonography

Holger R. Roth*, Jamie R. McClelland*, Darren J. Boone†, Marc Modat*, M. Jorge

Cardoso*, Thomas E. Hampshire*, Mingxing Hu*, Shonit Punwani†, Sebastien

Ourselin*, Greg G. Slabaugh**, Steve Halligan† and David J. Hawkes*

*Centre for Medical Image Computing, University College London, UK

†Department of Specialist Radiology, University College Hospital, London, UK

**Medicsight PLC, London, UK

Abstract.

Purpose: Computed tomographic (CT) colonography is a relatively new technique for detecting bowel cancer or potentially precancerous polyps. CT scanning is combined with 3-dimensional image reconstruction to produce a virtual endoluminal representation similar to optical colonoscopy. Because retained fluid and stool can mimic pathology, CT data is acquired with the bowel cleansed and insufflated with gas and patient in both prone and supine positions. Radiologists then match visually endoluminal locations between the two acquisitions in order to determine whether apparent pathology is real or not. This process is hindered by the fact that the colon, essentially a long tube, can undergo considerable deformation between acquisitions. We present a novel approach to automatically establish spatial correspondence between prone and supine endoluminal colonic surfaces after surface parameterization, even in the case of local colon collapse.

Methods: The complexity of the registration task was reduced from a 3D to a 2D problem by mapping the surfaces extracted from prone and supine CT colonography onto a cylindrical parameterization. A non-rigid cylindrical registration was then performed to align the full colonic surfaces. The curvature information from the original 3D surfaces was used to determine correspondence. The method can also be applied to cases with regions of local colonic collapse by ignoring the collapsed regions during the registration.

Results: Using a development set, suitable parameters were found to constrain the cylindrical registration method. Then, the same registration parameters were applied to a different set of 13 validation cases, consisting of 8 fully distended cases and 5 cases exhibiting multiple colonic collapses. All polyps present were well aligned, with a mean ($\pm$ std. dev.) registration error of 5.7 ($\pm$ 3.4) mm. An additional set of 1175 reference points on haustral folds spread over the full endoluminal colon surfaces resulted in an error of 7.7 ($\pm$ 7.4) mm. Here, 82% of folds was aligned correctly after registration with a further 15% misregistered by just one fold.

Conclusions: The proposed method reduces the 3D registration task to a cylindrical registration representing the endoluminal surface of the colon. Our algorithm uses surface curvature information as a similarity measure to drive registration to compensate for the large colorectal deformations that occur between prone and supine data acquisitions. The method has the potential to both enhance polyp detection and decrease the radiologist's interpretation time.

1. INTRODUCTION

1.1. Motivation

Colorectal cancer is the second-largest cause of cancer mortality in the West, responsible for more than 1 million cases and 639 000 deaths each year[1]. Early detection and removal of potentially precancerous polyps (adenomas) arising from the endoluminal colonic surface has been shown to significantly reduce the incidence of subsequent colorectal cancer and thus mortality[2]. Optical colonoscopy (insertion of a video-endoscope into the cleansed colon) is the reference-standard whole-colon diagnostic test and combines diagnosis and treatment (since polyps can be removed). However, the procedure is uncomfortable for the patient, technically difficult to perform, and is occasionally associated with significant adverse events, including colonic perforation[3].

Computed tomographic (CT) colonography (CTC) is a relatively new alternative technique for imaging the colorectum which has been shown in large comparative studies to be as sensitive as colonoscopy for larger polyps and cancer[4,5]. Moreover, studies have shown CT colonography to be more acceptable to patients than colonoscopy[6], and to be relatively safe[7]. As for colonoscopy, the patient usually undergoes full cathartic bowel preparation prior to imaging. Subsequently, multi-detector helical CT is carried out with carbon dioxide colonic insufflation of the bowel (via a small rectal catheter) to maximize the attenuation contrast between the endoluminal surface and the colonic lumen. Image rendering software is used to reconstruct a 3-dimensional representation of the endoluminal bowel surface; hence the alternative title, *virtual colonoscopy*[8]. However, residual stool and fluid (or even normal anatomical variants) can sometimes look like polyps, and some regions of bowel may be under-distended, which impairs image interpretation by radiologists. To counteract this, it is standard practice to image the patient in two positions - prone and supine - which redistributes gas and residue within the colon[9]. By comparing corresponding regions from prone and supine datasets, the radiologist can assess whether a potential abnormality perceived on one dataset is a real polyp (i.e. its position remains the same, indicating fixation to the bowel wall) or retained stool (i.e. it moves). However, the colon is a relatively long tubular structure that is loosely attached to the abdominal wall via variable mesenteric attachments. The result is that the colon often undergoes considerable deformation during patient repositioning[10], or even severe local under-distension which can lead to colonic collapse. This complicates the interpretation task; identifying corresponding regions of endoluminal surface between prone and supine acquisitions is difficult, prolongs reporting time, and may lead to errors of interpretation. A reliable method for establishing spatial registration between the prone and supine CT colonography datasets has the potential to simultaneously improve diagnostic accuracy and reduce interpretation time. Furthermore, its result could be incorporated in computer-aided detection (CAD) algorithms in order

to improve their robustness and accuracy.

1.2. Related work

The earliest attempt at prone-supine registration involve identifying similar distances along an extracted centerline of the segmented colon in both datasets [11,12,13,14,15]. This line represents the virtual path through the center of the virtual colonic lumen, from anus to cecum. Methods involve linear stretching and shrinkage of the extracted centerlines based on relative path geometries (for example, local maxima on each centerline's axial coordinate as tie points). Some centerline-based methods can still be effective with colons exhibiting sections of colonic collapse where the segmented colon is disconnected, e. g. [13,15].

However, these methods provide only one degree of freedom relative to the colonic surface and so can only account for local stretching and shrinking along the length of the colon – they cannot account for torsion or other deformations 'around' the colon. Hence, they do not account for all the detailed deformation of the colon surface that we are interested in that commonly occurs between prone and supine positioning such as colonic torsion. Furthermore, aligning the centerline between the prone and supine images is restrained to establish the correspondence between the global shapes of the colon between both views. This shape can vary greatly when the patient changes positions and centerline-based methods might experience difficulties.

Alternatively, Näppi [16] defined several anatomical landmarks, using these to align the two datasets. Anatomical locations that are relatively resistant to deformation, such as the anus or colonic flexures, were identified. Other landmarks, including the cecum and recto-sigmoid junction, were inferred relative to the landmarks already defined. However, identification of a limited number of corresponding points is likely to be insufficient to describe the complex colonic deformations that occur when moving between prone and supine positions.

Other feature-based methods account for colonic rotation by using the teniae coli (three discrete muscles running longitudinally along the exterior colonic surface) as an additional feature [17,18]. However, the teniae coli alone are difficult to extract robustly. As with centerline-based methods, they aim to match the global shape of the colon and then have to interpolate to the surface in order to estimate the deformation of the detailed surface structure.

A voxel-based approach has been developed by Suh et al. [19]. Initially, Suh's method involves rigid dataset alignment, based on the location of the anus and the flexures followed by generation of an initial deformation field using the centerlines. Level-set distance maps from the colonic surface are then used to drive a non-rigid registration. They reported an error of 13.77 ($\pm$ 6.20) mm for aligning polyps in 21 patients. In our experience such voxel-based approaches lack robustness as it is very difficult to adequately constrain the registration to prevent physically implausible deformations while still recovering the large and complex deformations that can occur.

They extended their method to handle cases with local colonic collapse where the segmentations are disconnected [20].

⁶⁹ Although they show promise in handling disconnected segmentations, the validation set was limited to 4 CTC cases

⁷⁰ with only one collapse in one view and fully connected colon segmentation in the other. A reported average registration

⁷¹ error of 30.1 mm for 4 polyps suggests limited accuracy. This may be due to their method of handling local collapses

⁷² which allows the colon to change its topology during the registration. This could cause different structures to appear

⁷³ similar to each other rather than correctly aligning the corresponding anatomical structures, e. g. a fold being flattened

⁷⁴ rather than shifted.

⁷⁵ Fukano et al.[21] aimed to establish correspondence between the detailed colon surface by matching haustral folds

⁷⁶ extracted from prone and supine data. Although haustral folds can be detected robustly, it is very challenging to

⁷⁷ establish their correct correspondence between both views as their results indicate. They report 65.1% of corresponding

⁷⁸ large haustral folds and 13.3% of small haustral folds being matched correctly.

⁷⁹ Recently, Zeng et al.[22] presented a method based on conformal mapping combined with feature matching in order

⁸⁰ to establish correspondences between the prone and supine surface. They detect four flexures and one teniae coli in

⁸¹ order to divide the colon surface into five segments and map each segment to a rectangle. Correspondence between

⁸² prone and supine surfaces is then established for each rectangular segment individually. Therefore the method relies

⁸³ on being able to accurately determine exactly the same segments on the prone and supine surfaces, which can be very

⁸⁴ difficult even for fully distended colons, and may not be possible for cases with local colonic collapse. Furthermore,

⁸⁵ they established correspondence between the mapped segments using only a sparse point set of features extracted from

⁸⁶ some 'prominent' haustral folds, which are unlikely to provide an accurate alignment of the detailed colonic surface.

⁸⁷ Despite these drawbacks, they report promising results with an average 3D error of 5.65 mm using 20 validated pairs

⁸⁸ of polyps over 6 patients and a average 3D error of 7.51 mm using feature points.

1.3. Proposed solution

⁹⁰ The difficulties described in the previous sections motivated us to develop a method that simplifies the task of

⁹¹ establishing full spatial correspondence between prone and supine endoluminal colon surfaces. Since the colon is an

⁹² extremely flexible structure, the registration task requires a non-rigid transformation but should preserve the topology

⁹³ of the colonic wall. Our method reduces complexity by using cylindrical 2D representations of the endoluminal surface

⁹⁴ extracted from both prone and supine CTC datasets. This enables us to account for the large deformations and twisting

⁹⁵ that are inevitable between the two positions in 3D as relatively simple deformations of the cylinder.

⁹⁶ Topologically, the colon is an open-ended cylinder or tube. Hence, any position within the colon can be mapped by

⁹⁷ two indices: length along the cylinder and angular position. Each 2D point $p(x,y)$ on the cylindrical representation

⁹⁸ corresponds directly to a 3D point $s(x,y,z)$ in the CTC data. Any measure acquired in 3D and on the surface can be

⁹⁹ assigned to a corresponding 2D point p which can be used to drive registration. We propose the use of conformal

mapping of the endoluminal colonic surfaces from prone and supine CT colonography to obtain a 2D cylindrical representation. A shape measure is assigned to each 2D point p in order to drive a non-rigid cylindrical registration in the parameterized cylindrical space. This simplifies the registration task compared with full 3D volume registration. This registration is represented as a transformation between two cylinders that includes non-linear stretch along the colon, local rotation and local torsion. We propose a cylindrical implementation of the well-known B-spline registration method[23] in order to achieve this for fully connected colon and in the case of local colonic collapse.

A similar cylindrical B-spline transformation model was recently proposed by Huysmans et al.[24] in order to produce active shape models of tubular structures (e.g. clavicles, tracheae, and thrombi). Although the transformation model is very similar to the one used in this paper, their application is very different (they are trying to determine correspondence for a large population of shapes), and as such their method of assessing correspondence (the minimum description length of the resulting shape model) and their overall framework for performing the registrations cannot be used for registering prone and supine colonic surfaces.

We claim novelty for the first use of a cylindrical non-rigid registration method to align image derived representations of the full colon endoluminal surface in order to establish a correspondence between colon surfaces extracted from prone and supine CTC. Our motivation is to simplify the radiologist's task in interpreting the two datasets, in particular the assessment of possible polyps in the two views, to reduce the incidence of false positives, speed up interpretation and finally to provide correspondence in emerging computer assisted detection (CAD) applications that merge prone and supine datasets in order to reduce false positive detection rates.

2. METHODS

Each surface point on the endoluminal colon surface S can be described with two indices x and y using a cylindrical representation. Here, x denotes a position along the length of the colon and y its angular orientation. Several groups have proposed methods to "unwrap" or "virtually dissect" the colon in order to produce flattened 2D images of the endoluminal surface, which were developed to facilitate more rapid interpretation[25].

Conformal maps are typically applied to surface mesh triangulations in order to find a simpler representation of the three-dimensional object. They provide a one-to-one mapping of a 3D surface to 2D space while preserving local angles[26]. These methods are based on differential geometry and ensure conformal mapping of the entire surface while preserving appearance of local structures, e.g. polyps and haustral folds.

Our registration approach is based on the following principle: a prone endoluminal colon surface S_p in $\mathbb{R}^3$ can be transformed using the one-to-one mapping f_p to a parameterization P_p in $\mathbb{R}^2$. The supine surface S_s is mapped to P_s through f_s, respectively. Here, $_p$ and $_s$ denotes prone and supine respectively. If the necessary transformation $\mathbf{T}_{cyl}$ between P_p and P_s can be determined, the transformation $\mathbf{T}_{ps}$ between the surfaces S_p and S_s follows as shown in

Fig. 1, where the principle is illustrated with the endoluminal colon surfaces extracted from prone and supine CT colonography.

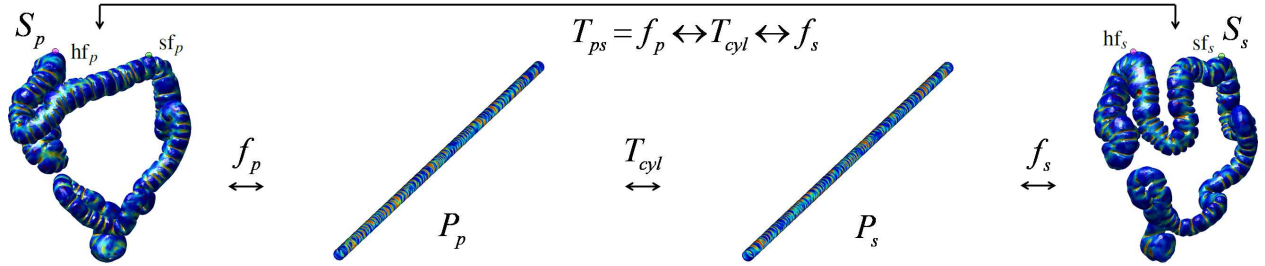$$T_{ps} = f_p \leftrightarrow T_{cyl} \leftrightarrow f_s$$

FIGURE 1. The principle of colon surface registration between prone and supine CTC using a cylindrical 2D parameterization (for patient 7), where the color scale indicates the shape index (see equation 2) at each coordinate of the surface computed from the 3D endoluminal colon surfaces. The hepatic and splenic flexures are marked as $\text{hf}_{p/s}$ and $\text{sf}_{p/s}$ respectively ($_{p/s}$ denotes prone/supine).

2.1. Colon segmentation

In order to extract the endoluminal colonic surface S, the inflated lumen L is segmented using the method described by Slabaugh et al.[27]. This method was developed for segmenting intraluminal gas over the entire colonic length. It is possible that gas-filled regions of small intestine are segmented as either isolated structures or connected to the colonic segmentation. Because we are only interested in the endoluminal surface of the colon, we reject all other objects by first eroding the segmentation with a spherical structure element with radius r to remove erroneous connections if necessary. Then the six-connected object with the largest volume is selected and subsequently dilated with a structure element of radius r in order to restore its original surface dimensions. Here, six-connected refers to an object in 3D voxel space which is only connected to direct neighboring voxels on its six sides. For this study, the radius r was adjusted interactively to produce the best segmentation by visual inspection. The parameter, r, ranged between 1 and 5 voxels for all our cases.

The rectal insufflation catheter (used to introduce the colonic gas necessary for luminal distension) is often excluded from the segmentation and can therefore lead to errors when extracting the endoluminal surface. We use a combination of morphological operations on a rectal region of interest in order to segment this plastic tube and add it to the colon segmentation L if necessary.

2.2. Topological correction

The colonic lumen L is now represented as a single six-connected object, ideally with a surface of genus zero which is topologically equivalent to a sphere. However, topological errors could be present in the segmentation due to noise

150 or reconstruction artifacts in the CT colonography data. This occurs particularly at adjacent folds or where the colon

151 folds back against itself, resulting in erroneous connections in the surface as shown in Fig. 2 (left).
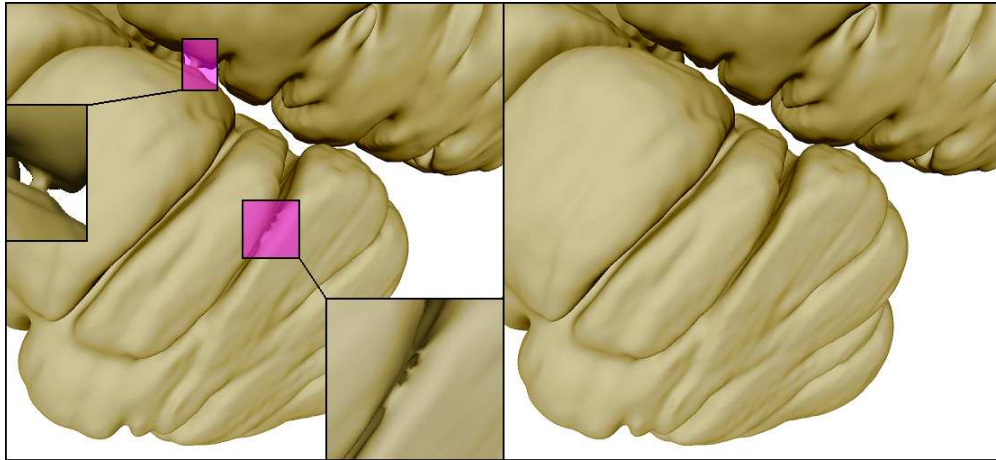

FIGURE 2.   Left: handles and an erroneous connection caused by limitation of the segmentation quality, resulting in incorrect topology. Right: the same surface region after topological correction.

152   We use a thinning algorithm [28,29] starting at the centerline (running at the virtual center of the colonic lumen from

153 cecum to rectum) and guided by a distance based priority map. This centerline can be extracted with the method

154 described by Deschamps et al. [30] based on evolving a wave front through the colon using the fast marching method [31].

155 This method of centerline extraction requires a defined start- and end-point. If the insufflation tube has been detected,

156 we use the most caudal point inside the tube. Otherwise the most caudal point in the colonic lumen L is used. This

157 corresponds to the patient's ano-rectal junction in both projections. A point in the cecum is currently selected manually.

158 Good correspondence for centerline start and end points is not essential for topological correction but improves rectal

159 and cecal mapping to a cylindrical representation as described in section 2.4.

160   The extracted centerline is used to generate an image C with each voxel on the centerline labeled as foreground.

161 A topology preserving region growing algorithm is then applied to the foreground of C maintaining its topological

162 characteristics. In this case, the centerline object is topologically equivalent to a sphere (genus zero). The region

163 growing will thus fill L whilst leaving voxels untouched which would introduce a topological change, e.g. handles.

164 This produces one-voxel-wide cuts through handles at the minimum distance position, resulting in a topologically

165 correct genus-zero segmentation L_{corr} of the endoluminal colon lumen (see Fig. 2).

166   2.3. Colonic surface extraction

167   The endoluminal colonic surfaces S are then modeled as triangulated meshes on the surfaces of L_{corr}, lying on the

168 gas-tissue border in the CTC images. Those surfaces are now guaranteed to be topologically correct (of genus zero).

169 In order to extract S we use the marching cubes algorithm on L_{corr} with a subsequent smoothing using a windowed

170   sinc function interpolation kernel[32]. This approximates a continuous surface which facilitates the convergence to a

171   2D parameterization using the Ricci flow method (as described in section 2.4). Furthermore, the mesh is decimated

172   using a quadric edge collapsing method[33] in order to reduce computation time. Finally, Loop's subdivision method[34]

173   is applied in order to achieve approximately uniformly sized and non-skewed faces over the entire surface S. This

174   procedure results in a simply connected genus-zero surface S of the colonic lumen L_{corr}. For all cases used in this

175   study, the surface meshes had typical edge lengths of 3.3 ($\pm$ 1.3) mm and about 60,000 faces.

2.4. Cylindrical representation of the endoluminal colonic surface

177   As described above, the endoluminal colon surfaces S can be modeled as piecewise-linear meshes composed

178   of vertices v_i that are connected using triangular faces. Those surfaces S can be parameterized using a discrete

179   conformal mapping method. One method to parameterize arbitrary discrete surfaces was introduced by Hamilton[35] for

180   Riemannian geometry based on Ricci flow. It deforms the surface proportionally to its local Gaussian curvature similar

181   to a heat diffusion process until it converges towards a desired Gaussian curvature[36]. Rather than mapping the surface

182   to a rectangle as with other methods[22], the Ricci flow does not require a border and therefore reduces distortion. Qiu

183   et al.[37] were the first to apply it to a colonic surface using volume rendering for the purpose of visualization, and

184   we follow their approach here with a small modification to the planar embedding (see below). We use Ricci flow to

185   produce a conformal mapping onto a 2D plane. The Ricci flow is defined as

$$\frac{d\mathbf{u}_i(t)}{dt} = \bar{K}_i - K_i, \tag{1}$$

186   where K_i is the Gaussian curvature at vertex v_i, $\bar{K}_i$ the desired Gaussian curvature and $\mathbf{u}_i$ a weighting function,

187   computed from a circle packing metric[36]. Ricci flow can be described as the gradient flow of an energy function[38]

188   which can be minimized using the steepest gradient descent method. For the purpose of parameterization of the colon

189   surfaces S in two-dimensional space, the target curvature K_i should be zero at all vertices v_i.

190   The original genus-zero surfaces S have to be converted to a surface SD of genus one[36] for this purpose, e.g.

191   converting a sphere-like surface to a torus-like surface. Therefore, we create holes in the surface mesh by removing

192   vertices and connected triangular faces closest to the previously selected cecal and rectal points. The remaining surface

193   is doubled, inverted and glued with the original mesh onto the vertices and edges along the previously produced holes

194   in a similar manner to[39]. The resulting surface SD is then parameterized using the Ricci flow while minimizing the

195   global maximum difference error between all current K_i and $\bar{K}_i$, E_{max}. This is computed until E_{max} convergence below

196   a pre-set value, resulting in a mesh P in $\mathbb{R}^2$ with two-dimensional coordinates of each surface location on S.

197   For all patients used in this study, the Ricci flow was minimized below an error of $E_{max} = 1e^{-6}$ which results

in a surface mesh with its local Gaussian curvatures K_i tending to zero everywhere. This mesh can be embedded into two-dimensional space $\mathbb{R}^2$ using the resulting edge lengths of each triangle, starting from a random seed face and then iteratively adding neighboring faces, in a similar manner to [36]. This is achieved by computing the position of each triangle vertex based on the intersection of two circles which have radii equal to the corresponding edge lengths. However, as K_i is not exactly zero at every vertex v_i, the resulting accumulated 2D mesh can have cracks and overlapping faces. These errors in computing the planar embedding P can be reduced if the Ricci flow converges towards smaller values of $E_{\max}$, but needs to be balanced against the computation time required for the Ricci flow. Segments of 2D surfaces, generated from the same endoluminal colon surface after convergence to different error levels $E_{\max}$, are shown in Fig. 3 (left, middle). However, if the errors in the planar embedding are small enough, the Ricci flow can be stopped and corresponding vertices of neighboring triangles can be joined together by averaging their two-dimensional positions. This results in a closed 2D mesh P without discontinuities as in Fig. 3 (right).
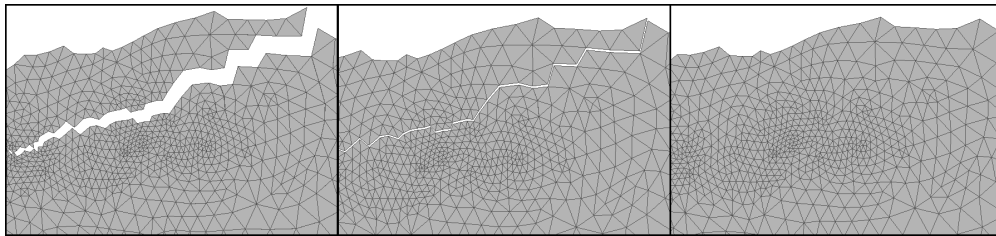

FIGURE 3. Computed planar embeddings P of the endoluminal colonic surface S with convergence errors $E_{\max} = 1e^{-4}$ (left), $E_{\max} = 1e^{-6}$ (middle) and the averaged planar embedding (right) with $E_{\max} = 1e^{-6}$.

The 2D mesh P represents a regular cylinder and can be re-sampled between 0 and $360°$ to generate rectangular raster images for use in the cylindrical registration as illustrated in Fig 4. Here, the horizontal dimension x corresponds to a distance along the colon from cecum to rectum and the vertical dimension y to the angular position around the circumference of the colon.
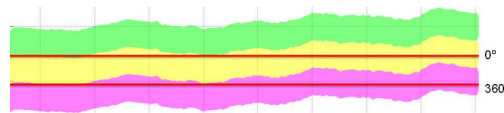

FIGURE 4. Sampling the unfolded mesh to generate rectangular raster-images I suitable for image registration. Each band represents a shifted copy of the planar embedded meshes P which are sampled between the horizontal lines to cover a full $360°$ of endoluminal colon surfaces S.

Sampling curvature information onto the parameterization P results in raster-images I for supine and prone endoluminal colon surfaces as shown in Fig. 5 (top, middle). The top and bottom edges of the images I correspond to the same point on the endoluminal colonic surfaces S, thus representing the endoluminal colonic surface as a cylinder.
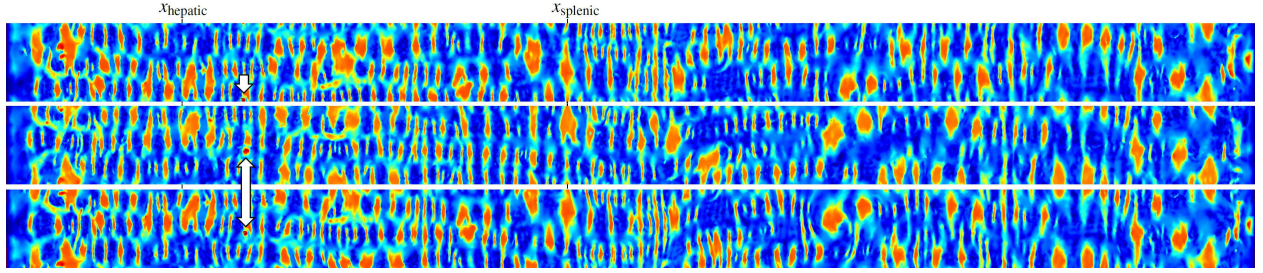
FIGURE 5. Supine (top), prone (middle) and deformed supine deformed to match prone (bottom) raster images of patient 7 where each pixel has the value of the corresponding shape index computed on the endoluminal colonic surface. The *x*-axis is the position along the colon, while the *y*-axis is its circumferential location. The *x*-positions for the detected hepatic and splenic flexures are marked as x_{hepatic} and x_{splenic}. The location of a polyp is marked before (top) and after registration (middle, bottom). Corresponding 3D renderings are illustrated in Fig. 1.

The chosen resolution ratio of 16 between $n_x = 4096$ and $n_y = 256$ corresponds approximately to the ratio between the length of the centerline and the average circumference around the colon. For all un-collapsed cases used in this study, the average length was 1.7 m and the average circumference was 10.8 cm, giving a ratio of 15.7.

For this resolution $n_x \times n_y$, any two neighboring pixels correspond to 3D points which are 0.27 (standard deviation 0.29) mm apart on average, with 99% of neighboring pixels being less than 1.2 mm apart. This suggest that, even though the circumference of the colon changes along its length, the distortion introduced by mapping S onto a cylindrical image I with constant width is sufficiently small enough over most of the endoluminal colon surface. Therefore, any 3D surface location on S can be interpolated with adequate accuracy. Furthermore, our experiments show that the distortion introduced by this step can be successfully recovered by our cylindrical non-rigid registration (as described in section 2.5).

Each pixel of I has a value assigned to it in order to drive a non-rigid registration. These values are estimated (using barycentric interpolation) from the local surface shape index (*SI*) computed on each vertex v_i of the three-dimensional surface S. The shape index *SI* is a normalized shape descriptor based on local curvature (see Fig. 6) and defined as

$$SI \equiv \frac{1}{2} - \frac{1}{\pi} \arctan\left(\frac{\kappa_1 + \kappa_2}{\kappa_1 - \kappa_2}\right), \qquad (2)$$

where the principal curvatures κ_1 and κ_2 are the maximum and minimum curvatures computed on the surface S[40].

The shape index represents the local topological shape of the surface S (as illustrated in Fig. 6). It is a good scalar measure for describing the local structures on colonic surfaces, such as haustra, folds and polyps. It can be also be used for polyp detection[41].
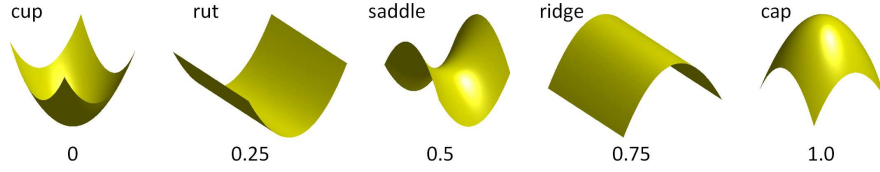
FIGURE 6. The shape index *SI* is a normalized shape measurement to describe local surface structures[41].

Corresponding features, like haustral folds, flexures or the teniae coli are clearly visible in both images of Fig. 5 (top, middle). These images are now aligned using a cylindrical intensity-based non-rigid registration method which will establish the full spatial correspondence between the endoluminal colon surfaces S_p and S_s.

2.5. Establishing spatial correspondence between prone and supine datasets

The two cylindrical representations are now in the same 2D domain but local structures are still misaligned. We will use a non-rigid registration method to align those local structures accurately. In order to provide good initialization for the registration algorithms, we use corresponding surface points at the hepatic flexure ($\text{hf}_{p/s}$) and splenic flexure ($\text{sf}_{p/s}$) to scale the 2D parameterizations linearly along the *x*-axis (using x_{hepatic} and x_{splenic}). The flexures are detected based on local maxima of the z-coordinate of the centerline. We detect the hepatic flexure as the first maximum, coming from the cecum, to be above t_{hepatic} of the maximum centerline z-coordinate. The splenic flexure is detected as the maximum which is the first to lie above t_{splenic} of the maximum centerline z-coordinate, relative to the rectum. In order to provide robustness against wrongly detected flexure correspondences, we discard flexures if their centerline distance vary by greater than t_{var} between prone and supine datasets. Based on our experiments, we found good parameters to be $t_{\text{hepatic}} = 60\%$, $t_{\text{splenic}} = 95\%$ and $t_{\text{var}} = 5\%$ for all cases used in this study. The corresponding *x*-positions for the hepatic and splenic flexures are marked as x_{hepatic} and x_{splenic} in Fig. 5 after linear scaling along the *x*-direction.

The cylindrical representations are used to generate shape index images I_p and I_s, where each pixel corresponds to a position on the colon surface in 3D. We establish the alignment between I_p and I_s using a cylindrical non-rigid B-spline registration method. This method is developed from the 3D free form deformation based registration of Rueckert et al.[23] with the fast implementation provided by Modat et al.[42].

A standard (non-cylindrical) 2D cubic B-Splines deformation model uses a lattice of control points $\{\vec{\phi}\}$. The spacing between each control point is uniform and noted as δ_x and δ_y along the *x*- and *y*-axis respectively. For each pixel $\vec{x}$ in the domain Ω of the target image. the deformation $\mathbf{T}_{2D}(\vec{x})$ can be computed as:

$$\mathbf{T}_{2D}(\vec{x}) = \sum_{i,j} \beta^3 \left(\frac{x}{\delta_x} - i \right) \times \beta^3 \left(\frac{y}{\delta_y} - j \right) \times \vec{\phi}_{ij}, \tag{3}$$

where β^3 represents the cubic B-Spline function.

In order to account for the cylindrical nature of the registration we modified the transformation model in a similar

257   fashion to Huysmans et al.[24]. For standard B-spline registrations the control point grid must extend outside the image

258   by at least one control point spacing in each direction so that the deformation is defined over the whole image. For

259   the cylindrical registrations, the control point grid does not extend outside the images in the *y*-direction (around the

260   cylinder). Instead, when an extended control point is required, the corresponding value is taken from the opposite side

261   of the grid. Therefore the equation for the cylindrical deformation is:

$$\mathbf{T}_{\text{cyl}}(\vec{x}) = \sum_{i,j} \beta^3 \left(\frac{x}{\delta_x} - i \right) \times \beta^3 \left(\frac{y}{\delta_y} - j \right) \times \vec{\phi}_{ik}, \tag{4}$$

262   where the control point is indexed by k instead of j, and k is defined as:

$$k = \begin{cases} j + N_{\delta_y} & \text{if } j < 0 \\ j & \text{if } 0 \leq j < N_{\delta_y} \\ j - N_{\delta_y} & \text{if } j \geq N_{\delta_y} \end{cases} \tag{5}$$

263   Here, N_{δ_y} is the number of control points in the *y*-direction.

264   In addition we prevent any displacement in the *x*-direction (along the colon) at each end of the image by fixing the

265   *x*-displacement of the first and last three control points to be zero. This ensures that the ends of the images are aligned

266   with each other, while still allowing for twists around the colon.

267   The two cylindrical shape index images I_p and I_s are aligned by finding the transformation which maximizes the

268   objective function:

$$\mathscr{O}\left(I_p, I_s \left(\mathbf{T}_{\text{cyl}} \right); \{\vec{\phi}\} \right) = (1 - \lambda - \mu) C_{\text{similarity}} - \lambda C_{\text{smooth}}(\mathbf{T}_{\text{cyl}}) - \mu C_{\text{volpres}}(\mathbf{T}_{\text{cyl}}) \tag{6}$$

269   which combines a similarity measure, $C_{\text{similarity}}$, and two penalty terms, C_{smooth} and C_{volpres}, weighted against each

270   other by the user-specified weights λ and μ. The similarity measure used was the mean sum of squared differences

271   (mean *SSD*):

$$C_{\text{similarity}} = -\frac{1}{N} SSD = -\frac{1}{N} \sum_{\vec{x} \in \Omega} \left[I_p(\vec{x}) - I_s \left(\mathbf{T}_{\text{cyl}}(\vec{x}) \right) \right]^2. \tag{7}$$

272   where $N = n_x \times n_y$ is the number of pixels.

273   Two constraint terms were used to try and prevent unrealistic deformations. The bending energy describes the

274   smoothness of the deformation and is defined as:

$$C_{\text{smooth}} = \frac{1}{N} \sum_{\vec{x} \in \Omega} \left(\left| \frac{\partial^2 \mathbf{T}_{\text{cyl}}(\vec{x})}{\partial x^2} \right|^2 + \left| \frac{\partial^2 \mathbf{T}_{\text{cyl}}(\vec{x})}{\partial y^2} \right|^2 + 2 \left| \frac{\partial^2 \mathbf{T}_{\text{cyl}}(\vec{x})}{\partial xy} \right|^2 \right), \tag{8}$$

The volume-preserving penalty term discourages large expansions/contractions, and is defined as:

$$C_{\text{volpres}} = \frac{1}{N} \sum_{\vec{x} \in \Omega} \left[\log \left(\det \left(\text{Jac} \left(\mathbf{T}_{\text{cyl}} (\vec{x}) \right) \right) \right) \right]^2 \tag{9}$$

In addition we prevent folding occurring by introducing a folding correction scheme performed concurrently with the registration process[43]. For each voxel that corresponds to a negative Jacobian determinant we compute its influence on its neighborhood control points and change the control point positions until the determinant value is positive.

In order to find optimal parameters for the B-spline registration, we used a sub-set of the available cases for tuning the registration algorithm parameters. The following reported optimal parameters were found empirically by visual examination of the registration results and by assessing the alignment of polyps after registration.

We used a coarse-to-fine approach in order to capture first the largest deformations and then the smaller differences between both input images. This is achieved with a seven-level multi-resolution approach using I_p as target and I_s as source. Both the image and B-spline control point grid resolutions are doubled with increasing resolution levels. The final resolution level uses images with 4096×256 ($n_x \times n_y$) pixels. The control point spacing δ is 16 pixels in both directions at each resolution level. The gradient of the cost function is smoothed after each iteration, using a Gaussian kernel with a standard deviation of $3\,\delta$. Gaussian smoothing of the 2D images is applied at each resolution level with a standard deviation of two pixels. The objective function weights are set to $\lambda = 1e^{-4}$ and $\mu = 1e^{-4}$. These parameters were found to recover the majority of the deformation between the two images for the data used for tuning, while preventing unrealistic deformations from occurring.

The cylindrical B-spline registration results in a continuous transformation around the entire endoluminal colon surface and allows the mapping between S_p and S_s. From this mapping it is straightforward to determine the full 3D mapping $\mathbf{T}_{ps}$ (as shown in Fig. 1).

2.6. Dealing with collapsed colon

Despite adequate colonic insufflation, short segments of colonic collapse commonly occur, particularly when the patient changes position from supine to prone. Furthermore, residual colonic fluid due to suboptimal bowel preparation can occlude the colonic lumen, resulting in more than one colonic segment for 3D reconstruction. If the colon is locally severely under-distended, the segmentation method described in section 2.1 can lead to disconnected colon segments. Most 3D workstations allow the radiologist to manually choose the order in which the centerline connects these disconnected colonic segmentations. Fig. 7 shows a patient's colon with a collapse in the descending colon (DC) in the supine position. While some centerline-based methods can handle local colonic collapse, they only provide a 1D correspondence along the centerline. To the best of our knowledge, only Suh et al.[20] have attempted a 3D registration

³⁰³ of images where the colon is collapsed in only one view but report limited accuracy.

³⁰⁴   If the collapsed segment is relatively straight, its length can be estimated as the Euclidean distance between the

³⁰⁵ centerlines of the well-distended segments. The length of each well-distended segment is estimated based on the

³⁰⁶ length of its centerline. We currently select the beginning and end points, as well as the correct order of each segment,

³⁰⁷ manually. The angular alignment between each segment was determined as the shift around the y-axis which minimizes

³⁰⁸ the 3D distance between points with the same angular orientation on either side of the collapse. The cylindrical images

³⁰⁹ I of such a case (patient 17) are shown in Fig. 8. It can be seen that despite the missing data in the collapsed section of

³¹⁰ the descending colon, we can register both supine colon segments with the fully distended prone endoluminal colon
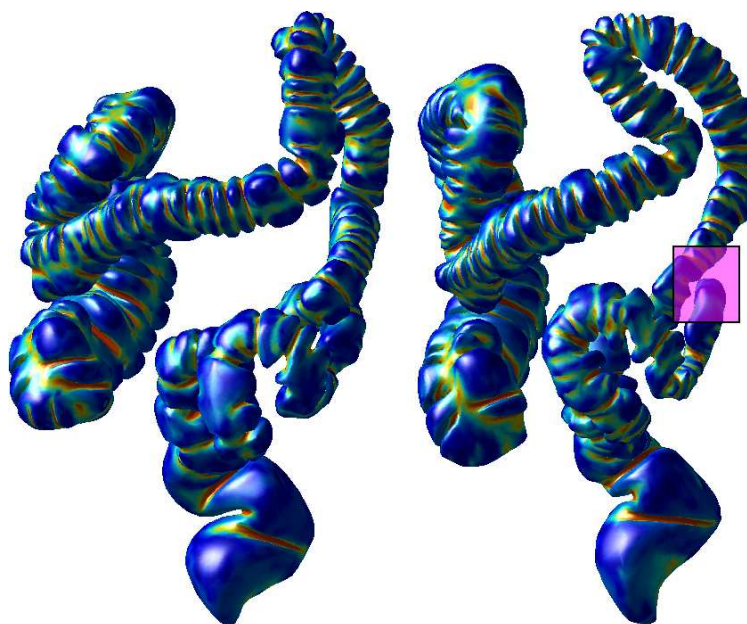
³¹¹ surface reasonably well.

FIGURE 7.   A case where the descending colon is collapsed in the supine position (marked, right image) but fully distended in the prone(left).
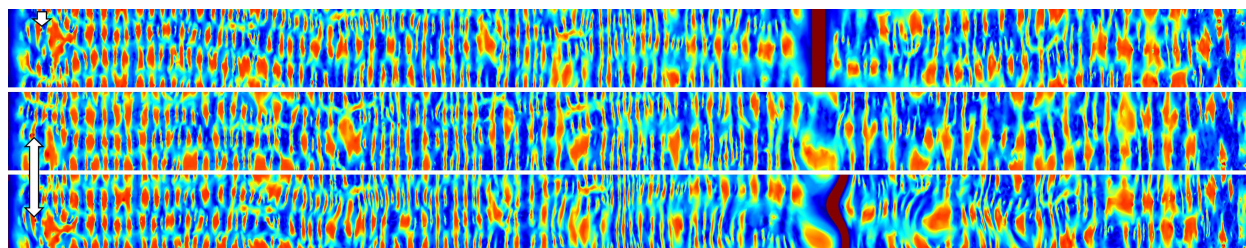

FIGURE 8.   Cylindrical representation as raster images of the collapsed supine (top), prone (middle) and deformed supine (bottom) endoluminal colon surface of patient 17. The location of a polyp is marked before (top) and after registration (middle, bottom).

3. CLINICAL EVALUATION

Ethical permission was obtained to utilize anonymized CT colonography data acquired as part of normal day-to-day clinical practice. CT colonography had been performed in accordance with current recommendations for good clinical practice[9] and any detected polyps subsequently validated via optical colonoscopy. For the purpose of establishing spatial correspondence across complete endoluminal surfaces, we selected 24 patients where the colon was not under-distended in both the prone or supine positions and who had either fluid 'tagging' (the increased radio-density allows 'digital cleansing' of residual fluid) or little remaining fluid. This allowed a continuous segmentation over the full length of the colon using the methods described in section 2.1.

The datasets were randomly allocated into development and validation sets (using random permutation), with 12 cases each. During the course of the development, we discovered that it is difficult to identify corresponding features by eye in the cylindrical image representations for some cases. Closer examination revealed that this was due to either large difference in distension of the colon in the prone and supine views or to insufficient fluid tagging. Large differences in distension can lead to considerable local dissimilarity of surface features, such as folds. Fig. 9 and 10 show such a case with marked differences in cylindrical representations I_p and I_s (Fig. 9, top and bottom), resulting from very different distensions (Fig. 10). These can occur only partially or over the full extent of the colon. Furthermore, differences in the colon surface can occur due to insufficient fluid tagging for accurate digital cleansing. This also leads to artifacts in the segmentation. We identified 4 development datasets with marked differences in local distension, which therefore had different surface features and these were excluded from the study, leaving 8 development cases (patients 1 to 8). The development set was used to tune the registration algorithm parameters (as described in section 2.5).
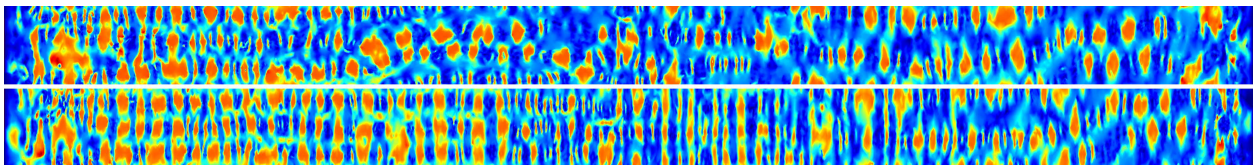

FIGURE 9. Widely different distension changes the shape index of the cylindrical representations in supine (top) and prone (bottom). 3D renderings are shown in Fig. 10
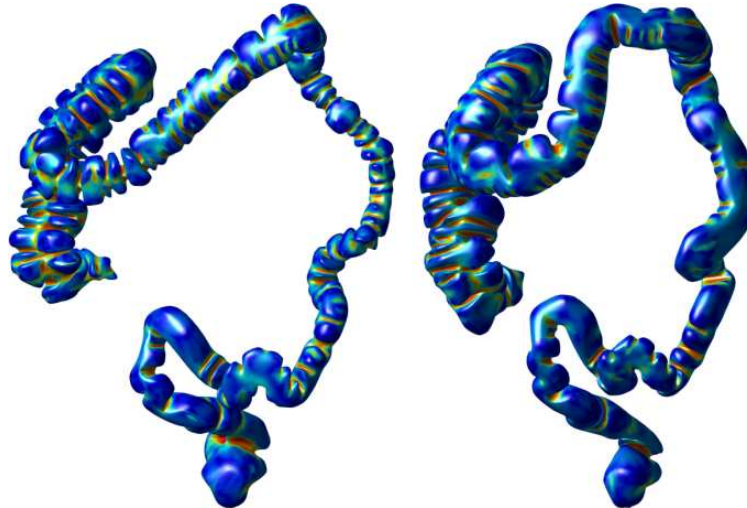
FIGURE 10. Different amounts of distension in prone and supine view cause differences of local features in the cylindrical images.

³³¹ Furthermore, this observation led us to exclude another 4 cases of the validation set which showed large differences

³³² in the cylindrical images. Of those, 2 showed marked differences in distension, 1 case showed insufficient fluid tagging

³³³ and 1 case showed both problems. This resulted in a total of 8 data sets with fully connected colon segmentations in

³³⁴ both views for validation (patients 9 to 16).

³³⁵ Recognizing the problems introduced by cases with marked differences in distension, we selected another 5 cases

³³⁶ for validation of the method on cases with local colonic collapse (patients 17 to 21). Here, the distension and surface

³³⁷ features of the 3D endoluminal surfaces S were judged by eye to be sufficiently similar in the well-distended segments

³³⁸ before execution of the registration algorithm. This selection process results in a total of 13 cases used for validation,

³³⁹ as described in the following sections: 8 fully connected sets and 5 with local colonic collapse. In order to assess the

³⁴⁰ spatial accuracy of the proposed registration method, we use clinically validated polyps and haustral folds to measure

³⁴¹ the registration error.

³⁴² 3.1. Validation using polyps

³⁴³ Experienced radiologists identified polyps in both prone and supine CT colonography scans using 2D multi-

³⁴⁴ planar reformats and endoscopy data for guidance. The polyps' endoluminal extent was labeled to provide reference

³⁴⁵ coordinates for validation. Polyp labels were checked and corrected if necessary and then matched by eye between the

³⁴⁶ prone and supine view by an experienced colonography radiologist (DJB).

³⁴⁷ The cases were selected to present a widespread distribution of polyps throughout the colonic length so that

³⁴⁸ registration accuracy could be investigated over the entire endoluminal surface. Crucially however, any polyps were

³⁴⁹ masked in the 2D cylindrical images I such that those pixels lying on or close to the polyp were ignored during

registration when computing the similarity measure $C_{\text{similarity}}$. Thus, it was impossible for the polyps used for validation to bias the registration results. Fig. 11 illustrates masking of polyps.
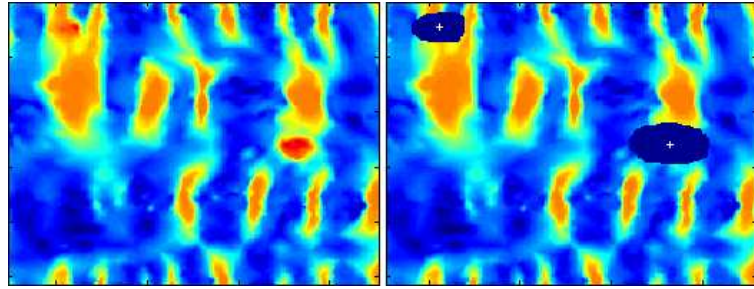

FIGURE 11. Masking of polyps to ensure they do not influence subsequent registration: polyps in unfolded view (left). Masked polyps (right) to be ignored in registration. The center of mass c which is used as a reference point is marked with a cross.

In order to determine registration error, we identified a pair of reference points for each manually matched polyp in the prone and supine views. The reference points were defined as the points at the center of the intersecting surface between the extracted endoluminal colon surfaces S and the segmented polyps. Therefore, these points lie on the surfaces S_{p} and S_{s} respectively. The center point $c(x,y)$ is computed as the center of mass of the intersecting pixels in the 2D images I, as indicated in Fig. 11 (right). Each 2D reference point $c(x,y)$ corresponds to a 3D point $c'_i(x,y,z)$ on the surfaces S which lies inside the polyp's volume. We then determined the registration error in mm by transforming each reference point c'_s on S_s using the 3D mapping $\mathbf{T}_{\text{ps}}$ to find $\mathbf{T}_{\text{ps}}(c'_s)$, which lies on surface S_{p}, and computing the 3D Euclidean distance to c'_{p}, which also lies on surface S_{p}.

All 8 datasets used to fine-tune the algorithm had clearly corresponding features in both prone and supine 2D representations, such as patient 7 in Fig. 5 (top, middle). It can be seen that after cylindrical B-spline registration, the corresponding features are well aligned (Fig. 5, bottom). The corresponding 3D renderings are illustrated in Fig. 1. Polyps of the same case and corresponding virtual endoscopic views after their prone and supine views were aligned using the registration result are shown in Fig. 12 and Fig. 13.
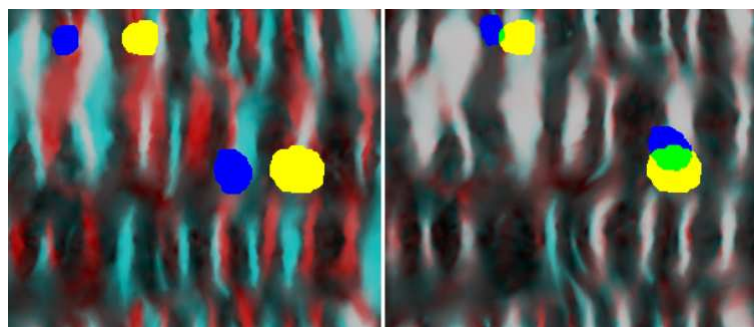

FIGURE 12. Overlay of masked out polyps before (left) and after (right) establishing spatial correspondence. The prone image is colored red with a yellow polyp mask, and the prone is colored cyan with a blue polyp mask. After establishing spatial correspondence, aligned features display gray and the overlapping region of polyp masks in green.
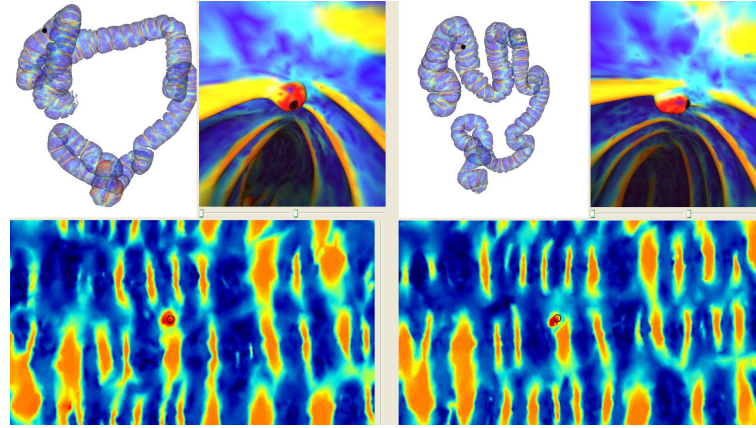
FIGURE 13. Polyp localization for patient 7 after registration using the prone (left) and supine (right) virtual endoscopic views. The black dot shows the resulting correspondence in the 2D (bottom) and 3D (top) renderings.

365   We used the same registration parameters as optimized using the development set (patient 1 to 8) on the validation set

366   (patients 9 to 21). Table 1 shows the results of assessing the registrations using the polyps of the 13 validations sets. The

367   error after the cylindrical parameterization but before the B-spline registration is denoted Polyp Parameterization Error

368   (*PPE*), and the error after the B-spline registration is denoted Polyp Registration Error (*PRE*). Before calculating

369   *PPE* the images are translated in the *y*-direction (around the colon) to minimize the *SSD* between the images, as the 0

370   degrees position is arbitrarily assigned by the cylindrical parameterization.

TABLE 1. Registration error in mm for 13 polyps in the 13 patients used for validation of the registration method. These included 8 fully connected cases (patients 9 to 16) and 5 cases with local colonic collapse (patients 17 to 19). The Polyp Parameterization Error (*PPE*) gives the error in aligning the polyps after cylindrical parameterization but before registration, the Polyp Registration Error (*PRE*) gives the error after cylindrical registration.

Patient	Polyp location	Collapsed location in prone	Collapsed location in supine	*PPE* [mm]	*PRE* [mm]
9	AC	none	none	32.4	3.0
10	Cecum	none	none	13.7	6.0
11	Cecum	none	none	30.2	3.1
12	Cecum	none	none	41.9	2.4
13	DC	none	none	15.7	6.8
14	AC	none	none	11.8	4.6
15	DC	none	none	23.9	3.6
16	AC	none	none	18.5	11.1
17	Cecum	none	1 x DC	24.8	9.4
18	AC	none	1 x SC	62.6	3.9
19	Rectum	1 x DC	1 x DC	55.9	6.0
20	Cecum	3 x (DC, SC)	none	13.3	12.4
21	AC	1 x DC	1 x DC	39.0	1.5
Mean [mm]				29.5	5.7
σ [mm]				16.4	3.4

371   The *PRE* had a mean (± std. dev.) of 5.7 (± 3.4) mm for 13 validation patients with a single polyp each, and all 13

372   polyps were well aligned. The *PPE* results show that cylindrical parameterization on its own is not enough to align the

373 datasets – the cylindrical non-rigid B-spline registration is required for accurate alignment. This result is sufficiently

374 accurate to direct the radiologist to an area of the endoluminal surface, which is close to the suspected lesion in both

375 views, even in the case of local colonic collapse (patients 17 to 21).

376 The hepatic flexure were not used to initialize the registration for patient 12 and patients 18-20, as the distances

377 along the centerline between prone and supine varied more than t_{var} (here, 5%). However, the cylindrical registration

378 was still able to align features well.

379 The resulting error for 9 polyps in the 8 development cases was 6.6 ($\pm$ 4.2) mm after non-rigid registration (*PRE*)

380 and therefore slightly higher than *PRE* of the validation set. The polyps for development of the registration method

381 occurred in the ascending colon (AC), transverse colon (TC), descending colon (DC) and sigmoid colon (SC).

3.2. Validation of spatial correspondence along the entire length of the colon

383 Polyps can give definite points of correspondence on the colon surface and give a good estimate of the registration

384 performance. However, their number is limited to only one polyp per case in our validation set. In order to assess

385 the registration quality over the entire endoluminal colon surface, corresponding haustral folds were chosen from the

386 prone and supine datasets. Reference point coordinates were provided to lie centrally on the fold in both views; the

387 haustral fold centers were automatically calculated by first segmenting each fold on the colon surfaces *S* using a graph-

388 cut method[44] based on the principal curvatures κ_1 and κ_2. Then, the center of each fold was computed as the vertex

389 which has the lowest maximum distance to any vertex on the border of the segmented fold.

390 Using the cylindrical representations to establish regions of likely correspondence and virtual colonoscopic views

391 for assurance, a radiologist (DJB, with experience in over 500 validated colonography studies) then manually identified

392 corresponding folds from the prone and supine views. Any folds where the radiologist could not be certain of

393 correspondence were not used for validation, but this still provided an average of 90 pairs of corresponding folds per

394 patient, with a total of 1175 pairs over all 13 validation cases (patients 9 to 21). The center points of the corresponding

395 folds were then used as corresponding reference points for assessing the registration.

396 Fig. 14 shows the normalized distributions of reference points versus a normalized position along the centerline

397 from cecum (0.0) to rectum (1.0) for 8 un-collapsed and 5 cases exhibiting local colonic collapse. The decline in

398 number of reference points is due to the fact that there are naturally fewer folds in the left hemi-colon.
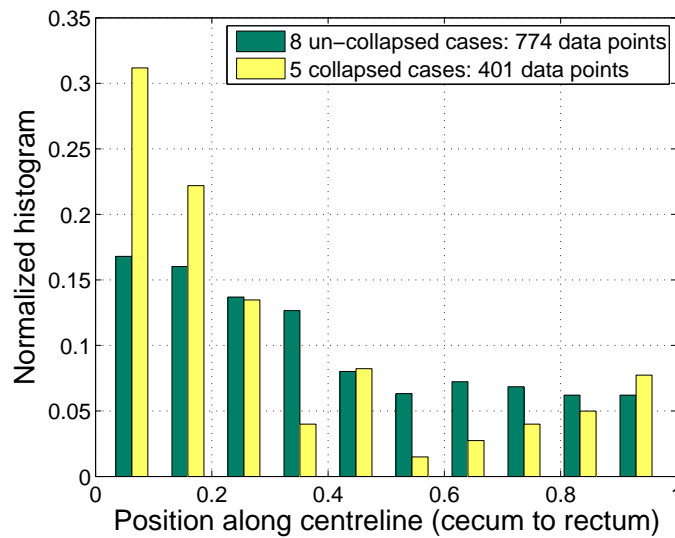
FIGURE 14. Normalized distributions of reference points normalized along the centerline from cecum to rectum for un-collapsed and collapsed cases.

We assess the Fold Registration Error (FRE) in the same way as described in section 3.1 but using the haustral fold centers as reference points. Using this large set of reference points, the FRE was 7.7 ($\pm$ 7.4) mm for a total of 1175 points distributed over all 13 validation patients. In comparison, just using the cylindrical parameterization on its own (before B-spline registration) a Fold Parameterization Error (FPE) results in an error of 23.4 ($\pm$ 12.3) mm. A histogram of the registration error (FRE) is shown in Fig. 15. Here, the normalized distributions of FRE for un-collapsed and collapsed cases are colored differently and displayed next to each other for comparison. It can be seen that the majority of points (95%) lie below an error of 22.8 mm, with a maximum error of 44.1 mm. However, the FRE is slightly higher for the 5 collapsed cases with 9.7 ($\pm$ 8.7) mm as opposed to the 8 un-collapsed cases with FRE of 6.6 ($\pm$ 6.3) mm.

Using our method haustral folds are almost always aligned with another haustral fold in the other image, but this is not always the correct corresponding fold. Using the segmented haustral folds we could analyze how many of the folds were aligned with the correct corresponding fold, and how many were misaligned by one or more fold. 82% of all 1175 reference points were assigned to the correct corresponding fold. 15% of reference points were misaligned by just one fold and 3% misaligned between two and three folds. This assumes that the radiologist correctly labeled corresponding haustral folds. We have no way to assess this but it is likely that at least some of the apparently misregistered data is due to this observer error. Nevertheless the identification of corresponding haustral folds is high.

In agreement with the FRE results, 71 % of haustral folds were correctly matched in the 5 cases with local colonic collapse. Whereas 88% of haustral folds in the 8 un-collapsed cases were assigned to the correct corresponding fold. The slight decline in registration quality of cases exhibiting local colonic collapse is due to the fact that, typically, the colon distension varies in the areas close to the collapse, e. g. the surface area of the descending colon in Fig. 7. Again,

₄₁₉ this introduces marked difference in the local surface features which degrades the registration accuracy in these areas.
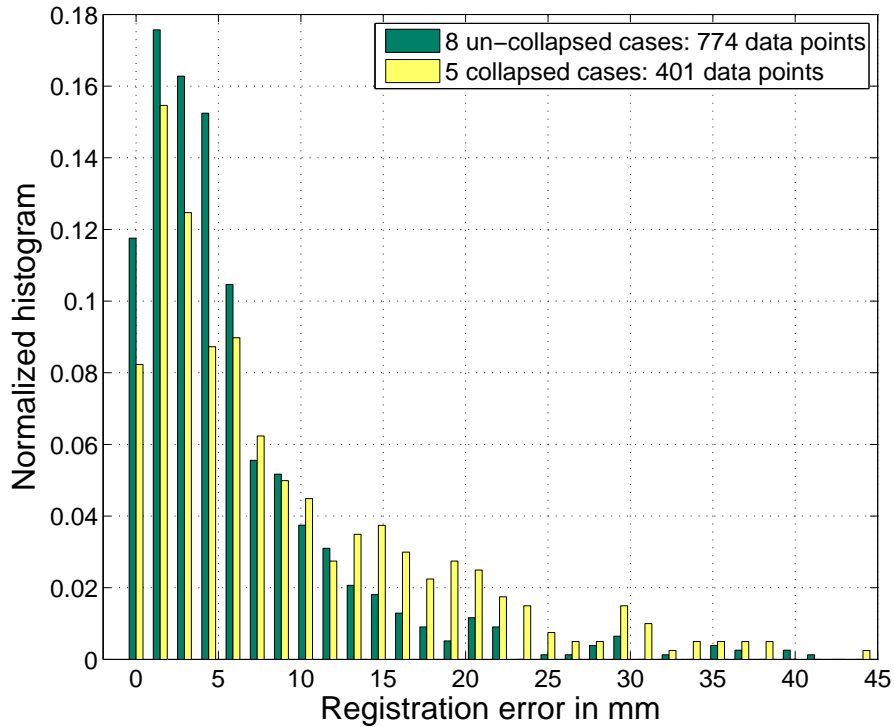

FIGURE 15. Normalized histograms of the Fold Registration Error (*FRE*) distributions in mm using reference points spread over the endoluminal colon surface for un-collapsed and collapsed cases.

4. DISCUSSION

₄₂₀ We have presented a novel method for establishing spatial correspondence between endoluminal colonic surfaces ex-

₄₂₁ tracted from prone and supine CT colonography data. Our method simplifies the problem of aligning the prone and

₄₂₂ supine surfaces from a 3D to a 2D task. This is achieved by mapping the full endoluminal surface to a cylindrical

₄₂₃ parameterization using a conformal mapping. The novel contribution of this work is that we use these cylindrical

₄₂₄ parameterizations in order to align the endoluminal colon surface using non-rigid B-spline registrations. Cylindrical

₄₂₅ raster-images with shape index values derived from the initial 3D surfaces are used to drive the registration. This

₄₂₆ process can establish accurate correspondence between the 2D cylindrical parameterizations, and hence give corre-

₄₂₇ spondence over the full 3D colonic surfaces which is able to recover the large colonic deformations and torsion that

₄₂₈ occurs between the two acquisition positions.

₄₂₉ Our approach is motivated by the assumption that the overall shape of the colon can undergo large deformations

₄₃₀ when the patient changes position, but that the local shape of surface structures, such as haustral folds, remains similar

enough between scans to align the surfaces. During the development of our method we discovered that for 8 of the 24 un-collapsed cases there were large regions where the surfaces structures appeared markedly different between the two scans. These were due to large differences in the distension of the colon or insufficient fluid tagging. We decided to exclude these cases from this study as we expect our current method to fail for such cases. However, we strongly suspect that most other methods presented in the literature that aim to generate accurate correspondence over the colonic surface (i. e. the feature based methods[22] and the voxel based methods[19,20]) will also experience difficulties with cases where the surface features appear differently in the two scans. The number of such cases observed in this study indicates that these cases are not infrequent, and methods that can address these cases must be developed to achieve maximum clinical benefit.

Another common occurrence is for there to be some regions of local colon collapse in one or both scans. Validation of our proposed registration method on 5 cases where there was a collapse in at least one view showed promising performance. It shows that the method is able to handle cases with multiple collapses in both views. Some of the centreline based approaches can handle regions of local collapse, but these only give approximate correspondence based on the shape of the centreline, and do not attempt to provide accurate correspondence over the colon surface. To the best of our knowledge there has only been one other method proposed to date that attempts to provide accurate correspondence over the colon surface (as opposed to just at the centreline) and to handle regions of local colon collapse[20]. However, this method has not yet been validated on cases with multiple collapses in both views as we have. Furthermore, their results show limited accuracy.

The method presented here relies on extracted colon surfaces of good quality. Therefore, pre-processing steps of segmentation (which involved manual interaction) and automated topological correction were necessary to extract topologically correct surfaces for the patient data used here. It is clear that obtaining good quality segmentations of the intraluminal colon surface reliably and robustly is a significant impediment to the clinical adoption of our method. We will therefore be devoting more resources to improving and automating our segmentations, both at the image analysis stage but also during patient preparation and data acquisition. Future work will extend the concepts described in this paper to cases of markedly different distensions between prone and supine colonography, insufficient tagging and automatically handling regions of local under-distension with more complex collapses. Although quality control of CT colonography is improving, these remain common problems in routine clinical practice.

The current method requires some manual interaction. These are: 1) choosing the structure element sizes interactively in order to correct the colon segmentations and include the the rectal insufflation catheter while visually inspecting the segmentation quality. 2) We selected the start and end-point as well as the correct order of each well-distended colon segment. Standard commercial 3D workstations already require the radiologist to manually choose the order of each colon segment. These steps are relatively quick to perform and require minimal manual input. Therefore we did not consider these few manual interactions to be a major impediment to our proposed method. However, We

will further investigate how individual colon segments can be arranged automatically in the case of colonic collapse. This will also incorporate methods of detecting two corresponding points at each segment which defined the start and end of each parameterized cylinder.

Given topologically correct surface meshes of the size used in this study, our single processor implementation of the Ricci flow conformal mapping (using the steepest gradient descent minimization) currently takes several hours to achieve sufficient convergence. However, faster solvers such as the Newton method [36] or a GPU-based implementation [37] can speed up the computation considerably. Alternatively, other conformal mapping methods could be used, e.g. [45] which require less computation time. It should be made clear that obtaining the cylindrical parameterization was not the focus of this study. There have been a number of parameterization methods presented in the literature, some based on conformal mappings [26,45,39] and some on other techniques [46], and we simply chose one that would generate an appropriate mapping for us to use. Future work will investigate faster implementation of the Ricci flow as well as alternative techniques for generating the cylindrical parameterizations, in order to produce appropriate parameterizations in a clinically feasible time frame.

In contrast to the cylindrical parameterization, the cylindrical B-spline registration, provides a result within a few minutes, which is fast enough to be clinically useful. A multi-resolution-level registration approach was used in order to help the registration optimization avoid getting stuck in local minima and to reduce the computation time. However, our validation shows that some haustral folds were misaligned by one or more folds indicating that the registrations were occasionally still getting trapped in local minima. Future research will investigate how better initialization of the cylindrical registration and/or a better choice of registration parameters could solve this problem.

In conclusion we have provided a framework for the alignment of information from prone and supine CT colonography; a very challenging registration problem. The method comprises conformal mapping of CT derived features onto a cylindrical surface, followed by a cylindrical registration of these features. This establishes an estimate of a dense correspondence throughout the derived colon surface. The results show promise, not only for polyp detection but also for establishing correspondence between corresponding haustral folds on a limited set of colonography datasets.

ACKNOWLEDGMENTS

REFERENCES

1. WHO. Cancer. `http://www.who.int/mediacentre/factsheets/fs297/en/`, Retrieved on February 20, 2011, February 2009.

2. W.S. Atkin, R. Edwards, I. Kralj-Hans, K. Wooldrage, A.R. Hart, J. Northover, D.M. Parkin, J. Wardle, S.W. Duffy, and J. Cuzick. Once-only flexible sigmoidoscopy screening in prevention of colorectal cancer: a multicentre randomised controlled trial. *The Lancet*, 375(9726):1624–1633, 2010.

3. V. Lohsiriwat. Colonoscopic perforation: Incidence, risk factors, management and outcome. *World Journal of Gastroenterology: WJG*, 16(4):425–430, 2010.

4. P.J. Pickhardt, J.R. Choi, I. Hwang, J.A. Butler, M.L. Puckett, H.A. Hildebrandt, R.K. Wong, P.A. Nugent, P.A. Mysliwiec, and W.R. Schindler. Computed tomographic virtual colonoscopy to screen for colorectal neoplasia in asymptomatic adults. *New England Journal of Medicine*, 349(23):2191–2200, 2003.

5. C.D. Johnson, M.H. Chen, A.Y. Toledano, J.P. Heiken, A. Dachman, M.D. Kuo, C.O. Menias, B. Siewert, J.I. Cheema, R.G. Obregon, et al. Accuracy of CT colonography for detection of large adenomas and cancers. *New England Journal of Medicine*, 359(12):1207–1217, 2008.

6. S.A. Taylor, S. Halligan, B.P. Saunders, P. Bassett, M. Vance, and C.I. Bartram. Acceptance by patients of multidetector CT colonography compared with barium enema examinations, flexible sigmoidoscopy, and colonoscopy. *American Journal of Roentgenology*, 181(4):913–921, 2003.

7. D. Burling, S. Halligan, A. Slater, M.J. Noakes, and S.A. Taylor. Potentially Serious Adverse Events at CT Colonography in Symptomatic Patients: National Survey of the United Kingdom. *Radiology*, 239(2):464–471, 2006.

8. H.M. Fenlon, D.P. Nunes, P.C. Schroy, M.A. Barish, P.D. Clarke, and J.T. Ferrucci. A comparison of virtual and conventional colonoscopy for the detection of colorectal polyps. *New England Journal of Medicine*, 341(20):1496–1503, 1999.

9. S.A. Taylor, A. Laghi, P. Lefere, S. Halligan, and J. Stoker. European Society of Gastrointestinal and Abdominal Radiology (ESGAR): consensus statement on CT colonography. *European Radiology*, 17(2):575–579, 2007.

10. S. Punwani, S. Halligan, D. Tolan, S.A. Taylor, and D. Hawkes. Quantitative assessment of colonic movement between prone and supine patient positions during CT colonography. *British Journal of Radiology*, 82(978):475–481, 2009.

11. B. Acar, S. Napel, DS Paik, P. Li, J. Yee, RB Jeffrey Jr, and CF Beaulieu. Medial axis registration of supine and prone CT colonography data. 3:2433–2436, 2002.

12. D. Nain, S. Haker, W.E. Grimson, E. Cosman, W. Wells, H. Ji, R. Kikinis, and C.F. Westin. Intra-patient prone to supine colon registration for synchronized virtual colonoscopy. *Medical Image Computing and Computer-Assisted Intervention – MICCAI*, pages 573–580, 2002.

13. P. Li, S. Napel, B. Acar, D.S. Paik, R.B. Jeffrey Jr, and C.F. Beaulieu. Registration of central paths and colonic polyps between supine and prone scans in computed tomography colonography: Pilot study. *Medical physics*, 31(10):2912–2923, 2004.

14. A.H. de Vries, R. Truyen, J. Van der Peijl, J. Florie, R.E. van Gelder, F. Gerritsen, and J. Stoker. Feasibility of automated matching of supine and prone CT-colonography examinations. *British Journal of Radiology*, 79(945):740–744, 2006.

15. S. Wang, J. Yao, J. Liu, N. Petrick, R.L. Van Uitert, S. Periaswamy, and R.M. Summers. Registration of prone and supine CT colonography scans using correlation optimized warping and canonical correlation analysis. *Medical Physics*, 36(12):5595–5603, 2009.

16. J. Näppi, A. Okamura, H. Frimmel, A. Dachman, and H. Yoshida. Region-based supine-prone correspondence for reduction of false positive cad poly candidates in ct colonography. *Acadamic Radiology*, 12:695–707, 2005.

17. J. Lamy and R.M. Summers. Intra-patient colon surface registration based on teniæ coli. *SPIE Medical Imaging 2007: Computer-Aided Diagnosis*, 6514(1):65140C, 2007.

18. A. Huang, D.A. Roy, R.M. Summers, M. Franaszek, N. Petrick, J.R. Choi, and P.J. Pickhardt. Teniae Coli–based Circumferential Localization System for CT Colonography: Feasibility Study1. *Radiology*, 243(2):551–560, 2007.

19. J.W. Suh and C.L. Wyatt. Deformable Registration of Supine and Prone Colons for Computed Tomographic Colonography. *Journal of computer assisted tomography*, 33(6):902–911, 2009.

20. Jung W. Suh and Christopher L. Wyatt. Registration of prone and supine colons in the presence of topological changes. *SPIE Medical Imaging 2008: Physiology, Function, and Structure from Medical Images*, 6916(1):69160C, 2008.

21. E. Fukano, M. Oda, T. Kitasaka, Y. Suenaga, T. Takayama, H. Takabatake, M. Mori, H. Natori, S. Nawano, and K. Mori. Haustral fold registration in CT colonography and its application to registration of virtual stretched view of the colon. *SPIE Medical Imaging 2010: Computer-Aided Diagnosis*, 7624(1):762420.

22. W. Zeng, J. Marino, K. Chaitanya Gurijala, X. Gu, and A. Kaufman. Supine and Prone Colon Registration Using Quasi-Conformal Mapping. *Visualization and Computer Graphics, IEEE Transactions on*, 16(6):1348–1357, Nov.-Dec. 2010.

23. D. Rueckert, L.I. Sonoda, C. Hayes, D.L.G. Hill, M.O. Leach, and D.J. Hawkes. Nonrigid registration using free-form deformations: application to breast mr images. *Medical Imaging, IEEE Transactions on*, 18(8):712–721, aug. 1999.

24. T. Huysmans, J. Sijbers, and V. Brigitte. Automatic construction of correspondences for tubular surfaces. *Pattern Analysis and Machine Intelligence, IEEE Transactions on*, 32(4):636–651, 2010.

25. K. Johnson, C. Johnson, J. Fletcher, R. MacCarty, and R. Summers. CT colonography using 360-degree virtual dissection: a feasibility study. *AJR Am J Roentgenol.*, 186:90–95, 2006.

26. M.S. Floater and K. Hormann. Surface parameterization: a tutorial and survey. *Advances in multiresolution for geometric modelling*, pages 157–186, 2005.

27. G. Slabaugh, X. Yang, X. Ye, R. Boyes, and G. Beddoe. A Robust and Fast System for CTC Computer-Aided Detection of Colorectal Lesions. *Algorithms*, 3(1):21–43, 2010.

28. G. Bertrand and M. Couprie. Transformations topologiques discretes. *Géométrie discrete et images numériques, Hermes*, pages 187–209, 2007.

29. M. Couprie. Note on fifteen 2d parallel thinning algorithms. *Université de Marne-la-Vallée, IGM2006-01*, 2006.

30. T. Deschamps and L.D. Cohen. Fast extraction of minimal paths in 3D images and applications to virtual endoscopy. *Medical Image Analysis*, 5(4):281–299, 2001.

31. D. Adalsteinsson and J.A. Sethian. A fast level set method for propagating interfaces. *Journal of Computational Physics*, 118(2):269–277, 1995.

32. G. Taubin, T. Zhang, and G. Golub. Optimal surface smoothing as filter design. *Computer Vision ECCV*, pages 283–292, 1996.

33. H. Hoppe. New quadric metric for simplifying meshes with appearance attributes. *Proceedings of the Article on Visualization'99: celebrating ten years*, pages 59–66, 1999.

34. C. Loop. Smooth subdivision surfaces based on triangles. *Master's thesis, University of Utah, Department of Mathematics*, 1987.

35. R.S. Hamilton. Three-manifolds with positive Ricci curvature. *J. Differential Geom*, 17(2):255–306, 1982.

36. M. Jin, J. Kim, F. Luo, and X. Gu. Discrete surface ricci flow. *IEEE Transactions on Visualization and Computer Graphics*, 14(5):1030–1043, 2008.

37. F. Qiu, Z. Fan, X. Yin, A. Kaufman, and X.D. Gu. Colon Flattening with Discrete Ricci Flow. *MICCAI workshop*, pages 97–102, 2008.

38. B. Chow and F. Luo. Combinatorial Ricci flows on surfaces. *J. Differential Geom*, 63(1):97–129, 2003.

39. W. Hong, X. Gu, F. Qiu, M. Jin, and A. Kaufman. Conformal virtual colon flattening. *Proceedings of the 2006 ACM symposium on Solid and physical modeling*, pages 85–93, 2006.

40. J.J. Koenderink. *Solid shape*. Cambridge, Massachusetts: MIT Press, 1990.

41. H. Yoshida and J. Nappi. Three-dimensional computer-aided diagnosis scheme for detection of colonic polyps. *Medical Imaging, IEEE Transactions on*, 20(12):1261–1274, 2002.

42. M. Modat, G.R. Ridgway, Z.A. Taylor, M. Lehmann, J. Barnes, D.J. Hawkes, N.C. Fox, and S. Ourselin. Fast free-form deformation using graphics processing units. *Computer methods and programs in biomedicine*, 98(3):278–284, 2010.

43. M. Modat, J. McClelland, and S. Ourselin. Lung registration using the NiftyReg package. *Proceedings of MICCAI Medical Image Analysis for the Clinic: A Grand Challenge, EMPIRE10*, 2010.

44. Y. Boykov, O. Veksler, and R. Zabih. Fast approximate energy minimization via graph cuts. *Pattern Analysis and Machine Intelligence, IEEE Transactions on*, 23(11):1222–1239, 2002.

45. S. Haker, S. Angenent, A. Tannenbaurn, and R. Kikinis. Nondistorting flattening maps and the 3-D visualization of colon CT images. *Medical Imaging, IEEE Transactions on*, 19(7):665–670, 2000.

46. G. Wang, G. McFarland, B.P. Brown, and M.W. Vannier. GI tract unraveling with curved cross sections. *Medical Imaging, IEEE Transactions on*, 17(2):318–322, 2002.